JOURNAL OF CATALYSIS 144, 38–49 (1993)

CO_2-Reforming of Methane over Transition Metals

J. R. ROSTRUP-NIELSEN AND J-H. BAK HANSEN

Haldor Topsøe A/S, Nymøllevej 55, DK-2800 Lyngby, Denmark

Received October 15, 1992; revised March 29, 1993

Catalysts based on Ni, Ru, Rh, Pd, Ir, and Pt are compared for CO_2-reforming of methane by studying the equilibrium for methane decomposition, the activity for reforming, and carbon formation, as well as the selectivity for carbon formation. Replacing steam by carbon dioxide has no significant impact on the reforming mechanism. All catalysts show smaller equilibrium constants for methane decomposition than that based on graphite, the effect being largest for the noble metals. Ru and Rh show high selectivity for carbon-free operation, which can be ascribed to high reforming rates combined with low carbon formation rates. Similar high selectivity can be achieved with a sulfur-passivated nickel catalyst. © 1993 Academic Press, Inc.

1. INTRODUCTION

The conversion of methane into synthesis gas is usually carried out by the steam reforming process (*1*):

$$CH_4 + H_2O = CO + 3H_2 \quad (1)$$

$$CO + H_2O = CO_2 + H_2. \quad (2)$$

Steam may be replaced by carbon dioxide:

$$CH_4 + CO_2 = 2CO + 2H_2. \quad (3)$$

Reaction (3) is of industrial interest because of the lower H_2/CO ratio in the product gas. CO_2-reforming is being practised in industry in various processes (*2–4*). Recently, reaction (3) has attracted interest as a CO_2-consuming reaction (*5, 6*).

Reaction (3) was studied over a number of base metal catalysts by Fischer and Tropsch (*7*) in 1928. They found gas compositions corresponding to thermodynamics and nickel and cobalt were identified as the preferred catalysts. A study of the kinetics of reaction (3) was published in 1966 by Bodrov and Apel'baum (*8*). They studied the reaction on a nickel film at gradientless conditions and found that the data could be represented by a kinetic expression obtained for steam reforming under similar conditions on a nickel film (*9*). At low CO_2/CH_4 ratios, the rate was observed to decrease by a factor of 15–25.

Thermodynamic calculations (*10*) show that the carbon limits are approached when carbon dioxide is added to the reformer feed. With high CO_2-contents in the feedgas or when operating on carbon dioxide and methane alone, thermodynamics predict the formation of carbon:

$$CH_4 = C + 2H_2 \quad (4)$$

$$2CO = C + CO_2. \quad (5)$$

On nickel catalysts, this results in the formation of carbon whiskers via a mechanism involving dissolution of adsorbed carbon atoms in the nickel crystal and nucleation of the whisker from Ni-surfaces, probably close to the (111) plane (*11*). The high surface energy and elastic energy (*11*) of the whisker structure can explain the smaller equilibrium constants for the decomposition reactions of methane and carbon monoxide which are observed on nickel catalysts (*1*).

The rate of carbon formation was found to be far less on noble metals (*12*), which was ascribed to a smaller dissolution of car-

0021-9517/93 $5.00

bon into these metals. Also, for steam reforming of ethane, the noble metals showed less carbon formation than did nickel (*13*). Rhodium and ruthenium were found to be far more active than nickel (*14*), whereas platinum and palladium had an activity comparable to that of nickel (*14*).

Carbon-Free CO_2-reforming could be achieved by "ensemble control" on a partly sulfur-poisoned nickel catalyst (*15*, *16*), and recently carbon-free CO_2-reforming was reported on catalysts containing rhodium (*17*, *18*), iridium (*18*, *19*), and ruthenium (*18*, *19*). Vernon *et al.* (*18*) compared iridium with nickel, rhodium, ruthenium, and palladium and found carbon formation on nickel and palladium, but no further investigations were made to explain the different behaviour of the metals. This study compares various metals for CO_2-reforming using the methods for studying the equilibrium of the carbon forming reaction, the catalyst activity, and selectivity for carbon formation as reported earlier for nickel catalysts (*1*).

2. EXPERIMENTAL

2.1. Catalysts

A series of catalysts was prepared by impregnation of 4.3 × 4.3-mm cylinders of an alumina-stabilized magnesia support (Mg/Al = 7/1 atom/atom), having a surface area of 50 m^2/g. Due to the basic magnesia, the metals were mainly deposited close to the external surface of the cylinders. The average metal content of the catalysts was 0.9–1.4 wt%. In addition, a nickel-based catalyst containing 16 wt% Ni on a spinel ($MgAl_2O_4$) support was included in the study. The catalysts were reduced at 550°C in dry hydrogen for 4 h before use.

The metal surface area of the catalysts was determined by chemisorption of hydrogen sulfide as described earlier (*1*) (conditions: $H_2S/H_2 = 15 \times 10^{-6}$ vol/vol, 550°C, 100 h). The metal surface area was calculated by assuming a monolayer of 44.0×10^{-9} g S/cm^2 as observed for nickel (*1*). This was assumed close to the composition of the monolayers on the noble metals (*20*). The catalyst properties are summarized in Table 1.

TABLE 1

Catalyst Properties

Catalyst	Support	Metal content (wt%)	Metal surface area (m_2/g)	Salt used for impregnation
Ni-1	MgO	1.4	1.1	$Ni(NO_3)_2$
Ru	MgO	1.4	3.0	$Ru(Cl)_3$
Rh	MgO	1.1	2.2	$Rh(NH_3)_6(NO_3)_3$
Pd	MgO	1.2	1.4	$Pd(NH_3)_4(NO_3)_2$
Ir	MgO	0.9	1.3	$Ir(Cl)_3$
Pt	MgO	0.9	1.0	$Pt(NH_3)_4(NO_3)_2$
Ni-2	$MgAl_2O_4$	16.0	5.3	$Ni(NO_3)_2$

2.2. Activity Tests

Activity tests were carried out in a simple flow system, operated at atmospheric pressure, with a tubular fixed bed reactor of stainless steel placed in an oven. The internal diameter of the reactor was 6 mm, and a thermowell with external diameter of 2 mm was placed in the center of the reactor. The catalyst cylinders were crushed down to 0.3–0.5 mm fragments prior to the activity test. The amount of catalyst was in the range of 10–50 mg. It was diluted with inert spinel support (0.3–0.5 mm fragments) to achieve a bed height of 12 mm. The axial temperature gradient in the reactor was measured to be a maximum of 12 and 35°C/cm at reforming conditions at 500 and 650°C, respectively.

Feed gases (CH_4, CO_2, and H_2) were supplied from bottles. Water was supplied via a piston pump, an evaporator, and a pulse dampener. The water was purified by ion exchangers. The methane was of 99.9995 vol% purity. The mixed feed of steam, methane and hydrogen was passed over a Cu/ZnO catalyst at 280°C for final purification. By gas chromatography hydrogen, methane, or higher hydrocarbons could not be detected in the carbon dioxide feed, which also contained less than 50 vol ppb of sulfur. The carbon dioxide was used without purification.

The activity of the catalysts was measured at three different standard gas compositions as follows:

Feed flows (Nl/h)	H_2O/CH_4-reforming	CO_2/CH_4-reforming	CO_2/H_2-reverse shift
CH_4	4.0	4.0	0.0
H_2O	16.0	0.0	0.0
CO_2	0.0	16.0	16.0
H_2	1.6	1.6	1.6

The dry feed gas flows were metered by mass flow controllers. Water was metered by a burette. The conversion was calculated on basis of the feed flow rates and the dry exit gas composition as obtained by gas chromatography.

The conversion of methane in the H_2O/CH_4-reforming tests was calculated as

$$\text{conversion of } CH_4 = \frac{y_{CO} + y_{CO_2}}{y_{CH_4} + y_{CO} + y_{CO_2}}, \tag{6}$$

where y is the dry mole fraction in the exit gas.

The conversion of methane during CO_2/CH_4-reforming tests was calculated as

$$\text{conversion of } CH_4 = \frac{y_{H_2} + y_{CO} - FH_2IN/DFEX}{4y_{CH_4} + y_{H_2} + y_{CO} - FH_2IN/DFEX}, \tag{7}$$

FH_2IN: feed flow of hydrogen;

DFEX: total dry exit flow, calculated via the carbon balance.

The conversion of carbon dioxide during CO_2/H_2-reverse shift tests was calculated as

$$\text{conversion of } CO_2 = \frac{y_{CO}}{y_{CH_4} + y_{CO} + y_{CO_2}}. \tag{8}$$

The turnover frequencies, N, were calculated from the measured rates by using the metal surface areas shown in Table 1 and a site area of 6.5×10^{-2} nm^2 as for nickel (*1*).

2.3. Methane Decomposition Equilibrium

The apparatus for TGA (thermogravimetric analysis) and the experimental procedure were described earlier (*21*). Ca. 600 mg of whole cylinders was loaded in the 880-mg quartz basket. The equilibrium constant of the reaction $CH_4 = C + 2H_2$ was determined by interpolation from carbon forming rates and carbon gasification rates at CH_4/H_2 ratios close to the equilibirum point. The equilibrium constant was determined at 500, 650, and 750°C, respectively, on the same catalyst loading. The equilibrium point was determined in the sequence 750, 650, then 500°C.

The TGA apparatus was used also to study the rates of carbon formation at 500 and 650°C, respectively, in a gas mixture of 95 vol% CH_4 and 5 vol% H_2. The morphology of the carbon was studied by electron microscopy.

2.4. Selectivity Studies

The TGA apparatus used for selectivity studies was similar to that described above except that only one whole catalyst cylinder (ca. 100 mg) was placed in a very open quartz/inconel basket allowing good contact between gas and catalyst.

The following four gas flows of individual gases were mixed and led to the reactor:

CH_4, 20 Nl/h; CO_2, 20 Nl/h;
H_2, 1 Nl/h; N_2, 3 Nl/h.

The reactor was initially heated to 577°C in a mixture of 10 Nl/h of nitrogen and 1 Nl/h of hydrogen. Carbon dioxide was then added, followed by methane, and the nitrogen flow was reduced to 3 Nl/h. The temperature was then increased by 0.75°C/min. This increase of temperature was continued until either a weight increase of 1–4 mg was observed or until the temperature had reached 847°C.

The selectivity study also included the two nickel-based catalysts (Table 1) in a partially sulfided state. Prior to the selectivity test the catalysts were sulfided at 800°C in hydrogen containing 15 vol ppm of hydrogen

TABLE 2

Activities of Metals for Reforming and Reverse Shift Turnover Frequency, N (molecules site^{-1} s^{-1})

Exp. no.	Cat.	Metal surface area (m^2/g)	H_2O/CH_4-reforming 550°C	CO_2/CH_4-reforming 550°C	CO_2/H_2-reverse shift 500°C
30	Ni-1	1.1	2.6	1.9	5.3
28	Ru	3.0	8.9	2.9	8.7
36	Rh	2.2	8.1	1.9	5.4
33	Pd	1.4	1.6	0.18	8.0
32	Ir	1.3	4.5	0.44	8.6
35	Pt	1.0	2.0	0.36	7.2
37	Ni-2	5.3	4.2	2.70	3.9

sulfide for 100 h. These conditions result in a sulfur coverage of the nickel surface at equilibrium corresponding to 85% saturation (*1*).

3. RESULTS

3.1. Activity Tests

The results are summarized in Table 2 and in the Arrhenius plots in Figs. 1–3. It is evident that the results achieved at very high rates above 550–600°C are subject to transport restrictions. The data for steam reforming (Fig. 1 and Table 2) show the expected sequence (*14*) of activity:

$$\text{Ru, Rh} > \text{Ir} > \text{Ni, Pt, Pd.}$$

The replacement of steam by carbon dioxide results in a decrease of activity to an extent depending on the metal, as summarized in Table 2. The effect is less on nickel, corresponding to the observations of Bodrov and Apel'baum (*8*), than on the noble metals, meaning that the superiority of rhodium and ruthenium is less pronounced. This is illustrated in Fig. 3, summarizing the data for nickel and ruthenium. The data in Figs. 1–3 indicate no significant change in activation energy when replacing steam by carbon dioxide, nor the presence of a compensation effect.

The CO_2-reforming tests were carried out with or without addition of hydrogen to the

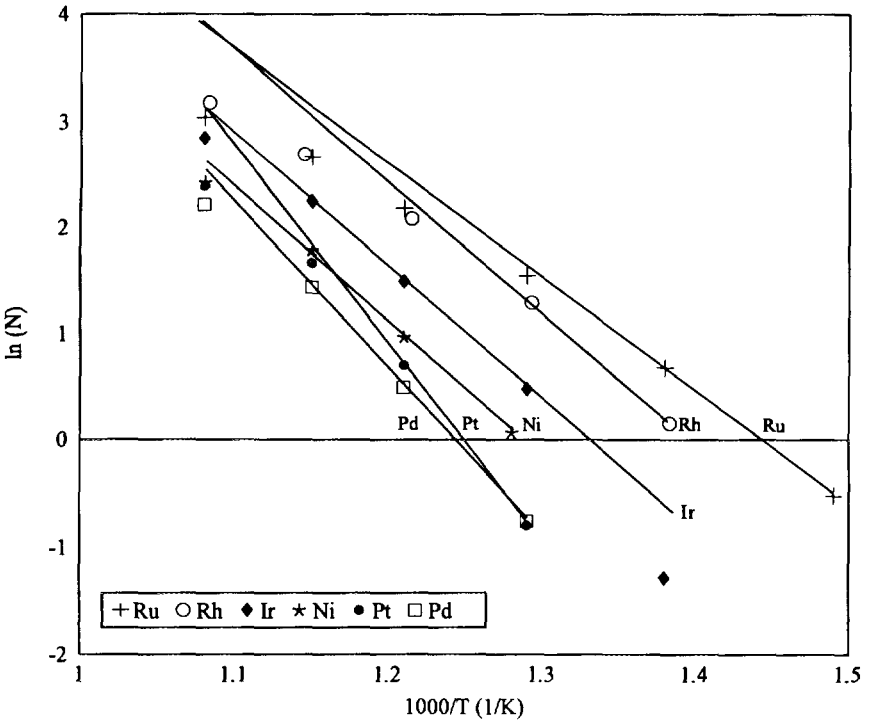

FIG. 1. Steam reforming rates: $H_2O/CH_4 = 4$ and $H_2O/H_2 = 10$.

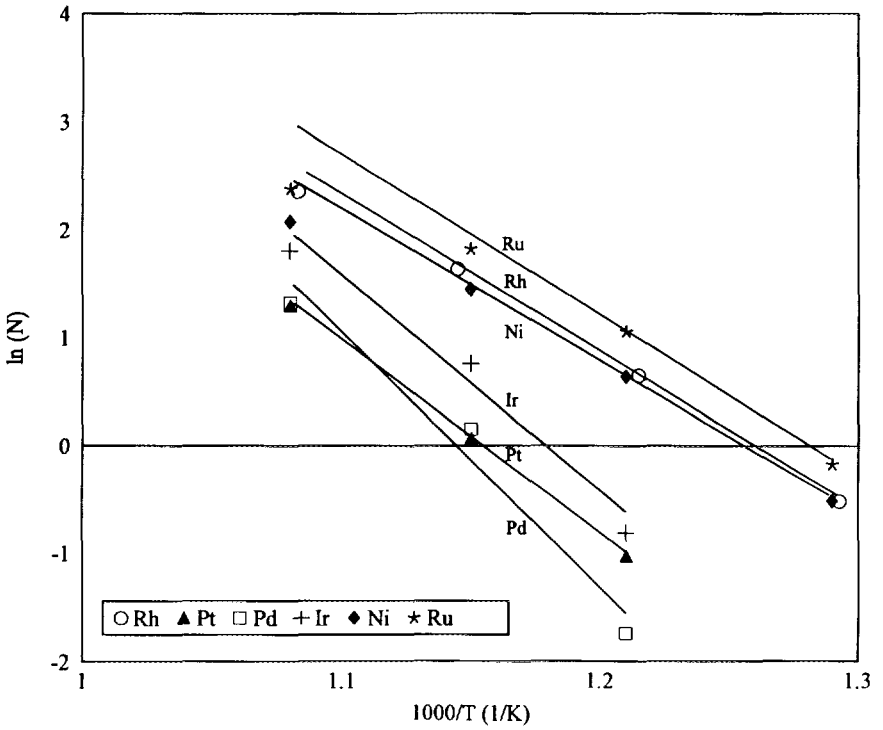

FIG. 2. CO_2-reforming rates: $CO_2/CH_4 = 4$ and $CO_2/H_2 = 10$.

feed ($CO_2/H_2 = 10$). The effect of hydrogen addition was insignificant. Other tests on nickel and ruthenium catalysts involved the variation of the steam partial pressure and the CO_2-partial pressure, respectively. For nickel, the reaction orders for steam and carbon dioxide were found to be ca. 1 and 0, respectively, for the reaction conditions close to the standard conditions. The CO_2-dependence appeared to be more complex over a wider range of CO_2 partial pressures. For the ruthenium catalyst, the reaction orders were found to be 0.3 and 0 for steam and carbon dioxide, respectively, for reaction conditions close to the standard conditions. At low CO_2/CH_4 ratios, the reaction order with respect to carbon dioxide approached one.

The rate of the reverse shift reaction (reverse (2)) was measured for all catalysts at $CO_2/H_2 = 10$ and with no methane in the feed. As shown in Table 2, all catalysts are very active including platinum and palladium having very low activities for the CO_2-reforming.

3.2. Methane Decomposition Equilibrium

The equilibrium constants resulting from the TGA experiments are shown in Fig. 4. All catalysts have equilibrium constants smaller than that calculated on a graphite basis. The Ni-a curve represents data from a commercial nickel catalyst published earlier (*22*) corresponding to a maximum nickel crystal size of ca. 300 nm. The Ni-b curve corresponds to a Ni/MgO catalyst prepared to achieve a maximum nickel crystal size below 10 nm. This results in a smaller equilibrium constant because of the higher surface energy of the whisker carbon. The noble metals have even smaller equilibrium constants. Palladium shows a track different from the other metals. The data for the Ni-1 catalyst at 750°C should be taken with some reservation. Due to very slow rates of both carbon formation and gasification, this equi-

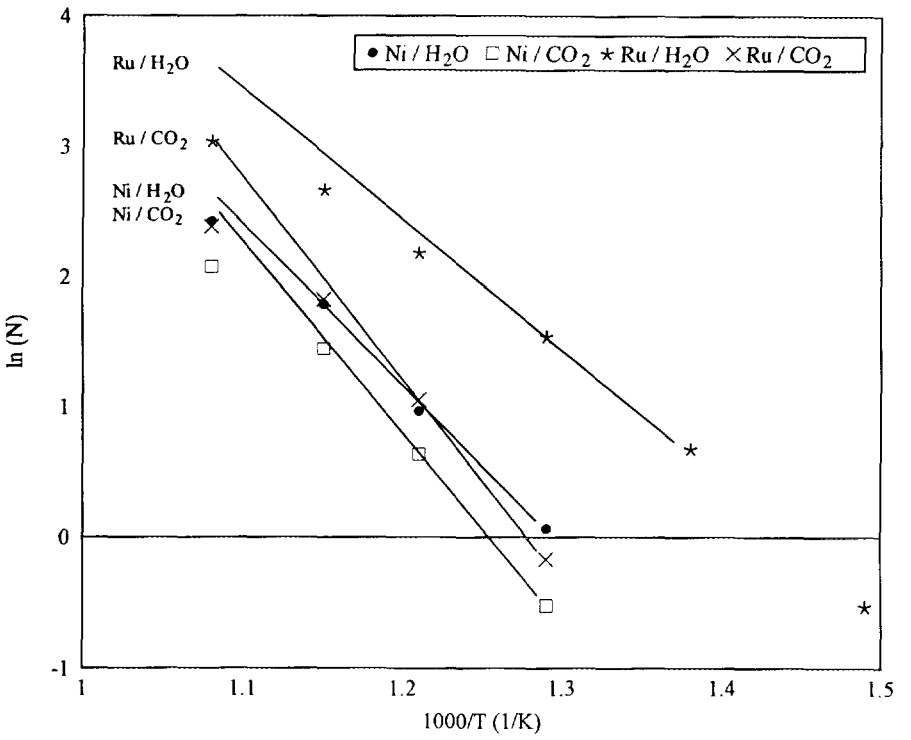

FIG. 3. Reforming rates for nickel (Ni-1) and ruthenium catalysts. Conditions as in Figs. 1 and 2.

libirum point was very difficult to determine.

The rates of carbon formation in the 95/5 vol/vol methane/hydrogen mixture are shown in Fig. 5. Nickel shows much higher carbon formation rates than the other metals, the differences being most significant at 500°C. Ruthenium has a low rate of carbon formation at 500 and 650°C, as well.

Electron microscopy was used to study the carbon morphology on samples on which 0.2–3.5 wt% of carbon had formed in 95/5 vol/vol of CH_4/H_2 at 500 and 650°C, respectively. The results are given in Table 3.

The noble metals, except for palladium at 650°C, did not form whisker (filamentous) carbon as observed on nickel. Whisker carbon was observed on the rhodium and platinum catalysts, but in both cases contamination of the catalyst with iron most probably caused the formation of whiskers. The carbon formed by the noble metals was of a structure which was difficult to distinguish from the catalyst structure. The ruthenium catalyst was examined by high-resolution electron microscopy and a structure was observed which resembled a few atomic layers of carbon, covering almost completely the catalyst surface (*23*). The carbon layers on the ruthenium catalyst are shown in Fig. 6.

3.3. Selectivity Tests

The results of the TGA tests studying simultaneously the CO_2/CH_4-reforming and the carbon formation are summarized in Table 4.

Carbon was formed rapidly on the nickel catalyst, whereas no carbon was formed on the ruthenium and rhodium catalysts. A rapid carbon formation occurred on the palladium catalyst at temperatures above approximately 600°C. A slow carbon formation was seen on the iridium and platinum catalysts at above approximately 750°C. Carbon-free operation was observed when

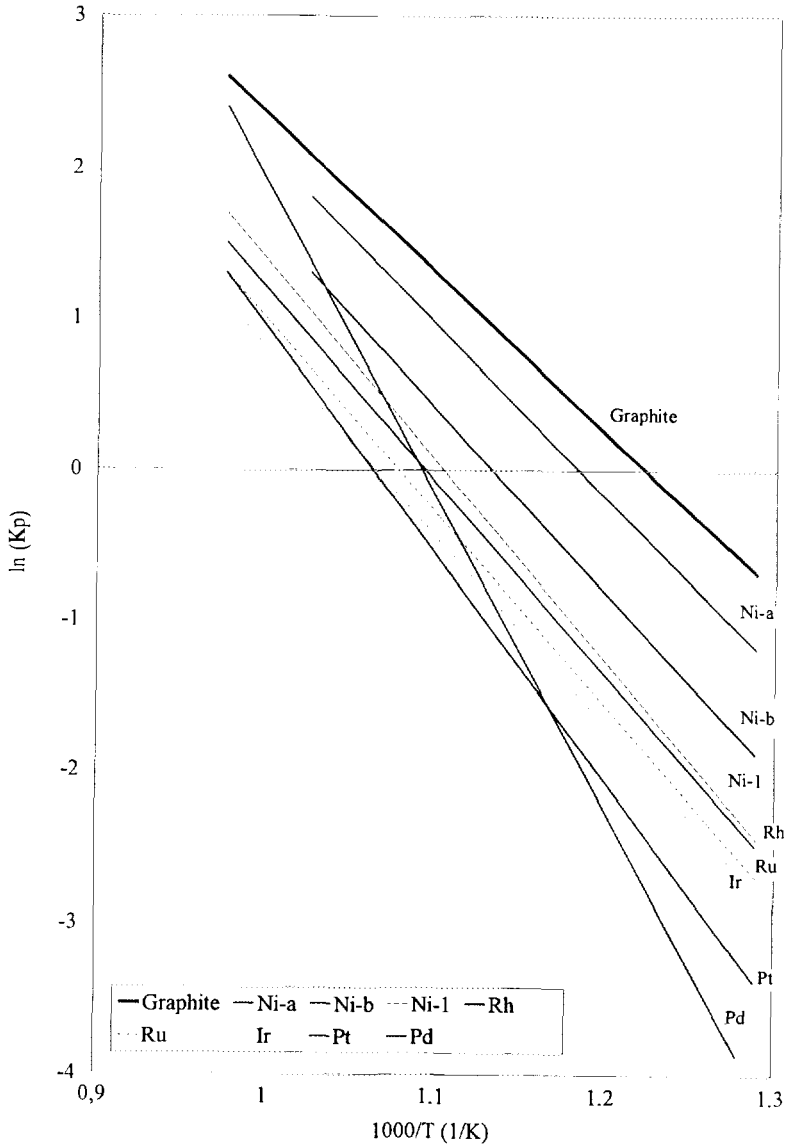

FIG. 4. Equilibrium constants for methane decomposition from TGA measurements.

using the nickel catalyst, Ni-1, after presulfiding at conditions resulting in an approximate sulfur coverage of 85%. This sulfur coverage has proven carbon-free operation in earlier reactor tests (*15*). The test of the fully impregnated nickel catalyst, Ni-2, showed carbon formation in the centre of the particle, as also observed earlier (*15*).

When the TGA unit was kept running at 847°C with the sulfur-passivated Ni-1 catalyst, carbon was indicated, probably because of the desorption of sulfur from the nickel surface.

The selectivity tests are characterized by conditions for kinetic competition. In the entire temperature range studied, the feed gas contains a large thermodynamic potential for formation of carbon via methane de-

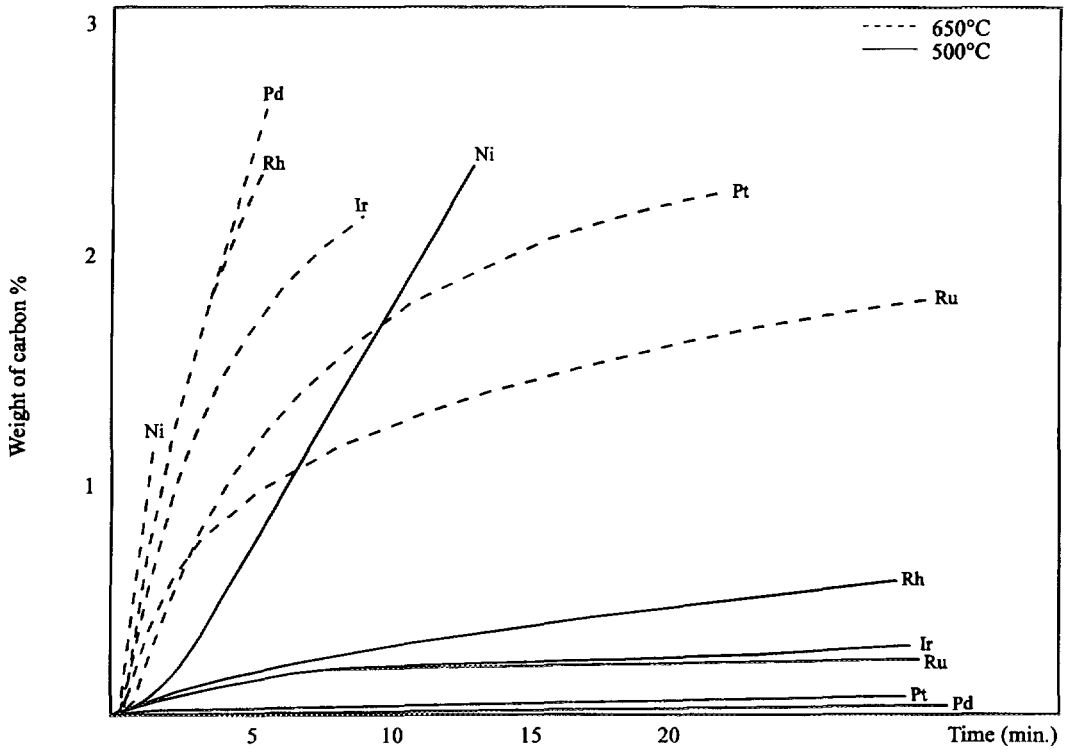

FIG. 5. Rates of carbon formation. CH_4/H_2 = 95/5. TGA measurements.

composition (reaction (4)), but the feed gas also contains a large thermodynamic potential for CO_2-reforming (reaction (3)).

The results obtained during the selectivity tests only give a rough order with respect to resistance towards carbon formation. The exact catalyst temperature and the exact gas composition in contact with the outer surface of the catalyst particle is in principle unknown because of the heat- and mass-transfer restrictions in the gas film around the particle. Consequently, catalysts of higher activity will be of lower temperature because of the endothermic CO_2-reforming reaction. Likewise, the outer surface of the catalyst of higher activity will be in contact with a more converted gas.

TABLE 3

Carbon Morphology

Catalyst	Temp. (°C)	Carbon (wt%)	Metal crystal size (nm)	Whisker diameter (nm)	Metal in whisker
Ni-1	500	3.5	5–20	5–20	Ni
	650	2.0	5–20	5–20	Ni
Ru	500	0.3	1.5–7	No whiskers	
	650	1.8	1.5–7	No whiskers	
Rh	500	1.1	1–10	No whiskers	
	650	2.5	3–100	10–30	Fe/Rh
Pd	500	0			
	650	2.8	10–25	10–25	Pd
Ir	500	0.5	<4	No whiskers	
	650	2.3	<4	No whiskers	
Pt	500	0.2	<3–4	10–15	Fe
	650	2.6	<3–4	10–15	Fe

Note. Carbon formed in CH_4/H_2 = 95/5 vol/vol at 500 and 650°C, respectively.

4. DISCUSSION

4.1. Kinetics

The kinetics for steam reforming depend on the type of catalyst (*1*, *14*), and probably the mechanism is changing with the temperature range in question. In conclusion, no general expression has so far been derived. The kinetics published by Xu and Froment

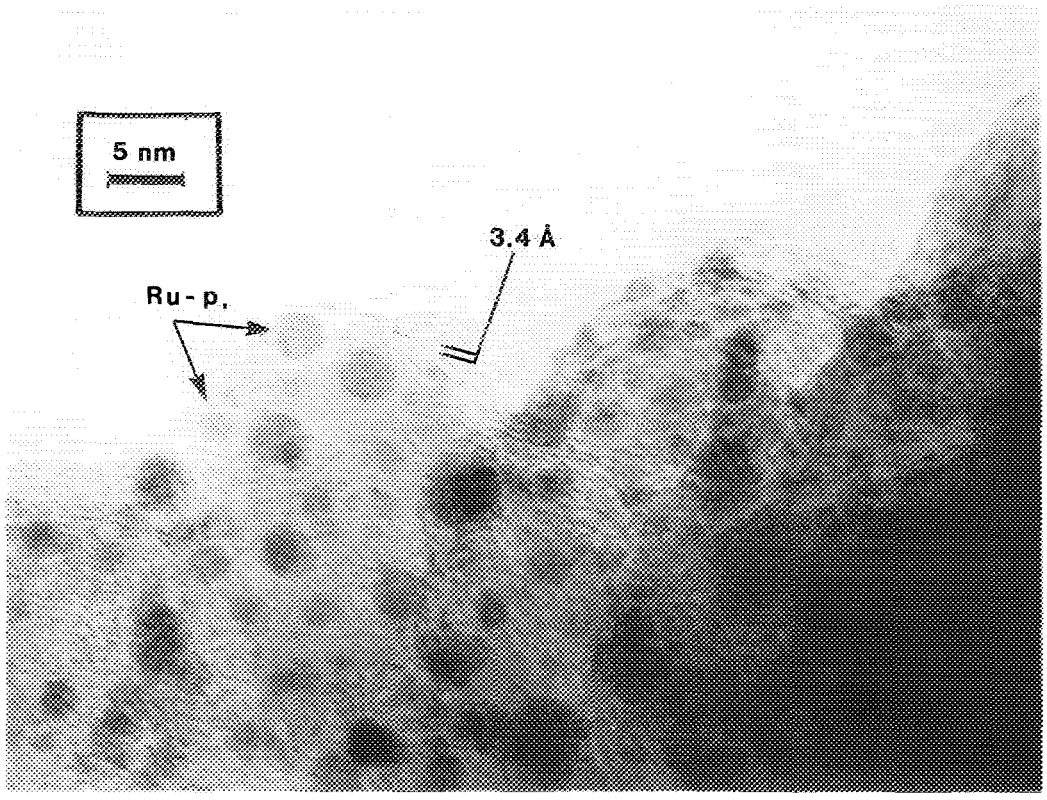

FIG. 6. Morphology of carbon deposits on ruthenium catalyst by high-resolution electron microscopy.

(*24*) were based on the Ni-b catalyst used in this study as well. The study included a large number of measurements, but within a narrow range of feed composition and temperature (H_2O/CH_4 = 3–5, T = 500–575°C). Using the rate equation on the data in this study, however, could not explain the observed decrease in rate, when replacing steam with carbon dioxide. On the contrary, the kinetics of Xu and Froment (*24*) predict an increase of rate at high temperatures (600°C). Although this can in principle be explained by a negative heat of adsorption for steam in the rate equation, a number of studies point to a positive heat of adsorption for steam on nickel (*1*, *9*, *25*, *26*).

TABLE 4

Selectivity Studies

Catalyst	Temp. interval for carbon formation (°C)	Temp. of termination of experiment (°C)	Total carbon formed (mg)	Conversion of methane at 800°C (%)
Ni-1	577–610	610	4.4	—
Ru	No carbon	847	0.0	7
Rh	No carbon	847	0.0	3
Pd	610–700	700	3.5	—
Ir	765–847	847	0.6	3
Pt	740–847	847	0.4	3
Ni-1 Sulfided	No carbon	847	0.0	0–1
Ni-2 Sulfided	740–769	769	1.2	0–1

Note. $CH_4/CO_2/H_2$ = 20/20/1 vol/vol. Temperature increase: 0.75°C/min from 577°C to a maximum of 847°C.

It is unlikely that the mechanism of CO_2-reforming differs significantly from that of steam reforming of methane. A simplified reaction sequence for the steam reforming may involve the following two irreversible steps, namely, the activation of methane as described by Alstrup *et al.* (*27*, *28*) followed by the surface reaction with adsorbed oxygen atoms:

$$CH_4 + * = CH_3* \rightarrow CH_2* \rightarrow CH* = C* \quad (9)$$

$$CH_x* + O* = CO + \frac{X}{2}H_2 + 2* \quad (10)$$

with the equilibrium step

$$H_2O + * = O* + H_2. \quad (11)$$

When adding carbon dioxide to the feed, the sequence should be supplemented by

$$CO_2 + * = O* + CO. \quad (12)$$

The decrease of rate when steam is replaced by carbon dioxide could in principle be explained by step (12) becoming rate determining, but this appears unlikely in view of the high rates for the reverse shift reaction on all catalysts and because the addition of hydrogen to the feed had little impact on the reaction rate on nickel and ruthenium.

It is more likely that the rates are influenced by the adsorption of carbon monoxide, the concentration of which is significant at CO_2-reforming conditions. Some of the tests were carried out close to the Boudouard equilibrium (reaction (5)). Under these conditions, the reaction sequence should be supplemented by

$$CO + * = CO* \quad (13)$$

$$CO* = C* + O*. \quad (14)$$

It is likely that C* may be less reactive than the CH_x* intermediates formed by activation of methane. This could explain the drastic decline in activity observed by Bodrov and Apel'baum (*8*).

The different behaviour of the metals when steam is replaced by carbon dioxide, shown in Table 2, is related to the size of the heat of chemisorption of carbon monoxide, as illustrated in Fig. 7. The metals which adsorb carbon monoxide more strongly (*29*, *30*) are the metals showing the largest decrease in rate when steam is replaced by carbon dioxide. However, more kinetic studies are required to support this explanation.

The change in mechanism when operating on carbon dioxide instead of steam would have little practical impact on reforming, because steam will be present not far from the inlet, and also in the centers of the catalyst particles, due to the low effectiveness in industrial reformers (*1*).

4.2. Carbon Formation

The morphology of carbon varies from metal to metal. As expected, no carbon whiskers were observed on the noble metals. It should be noted, however, that the formation of carbon whiskers on ruthenium and platinum has been reported by Baker and co-workers (*31*, *32*). The deviation from graphite data observed on the noble metals might be explained as for nickel as a contribution from surplus energy of the carbon structure, but further studies are required to clarify whether this effect is related to the metal crystal size.

The rates of carbon formation in CH_4/H_2 mixtures should be related to the different growth mechanisms with the dissolution precipitation mechanism for nickel enhancing rates, because of the high solubility of carbon in nickel. The behaviour of palladium might be related to the formation of an interstitial solid solution of carbon in palladium (*33*) and its mobility in palladium, as demonstrated by Ziemecki (*34*).

The shape of the curves in Fig. 5 for the noble metals may reflect a gradual deactivation. Whether this might be explained by the formation of encapsulating carbon, as indicated for ruthenium in Fig. 6, requires further investigation. This deactivation would have no consequence for practical CO_2-reforming because industrial reforming units should be operated at conditions with no potential for carbon formation (*1*, *10*).

4.3. Selectivity Tests

The results from the selectivity tests (Table 4) correspond to the observations in the activity tests and in the carbon formation tests. Ruthenium showing a high reforming activity (Table 2) and a low rate of carbon formation (Fig. 5) also shows high selectiv-

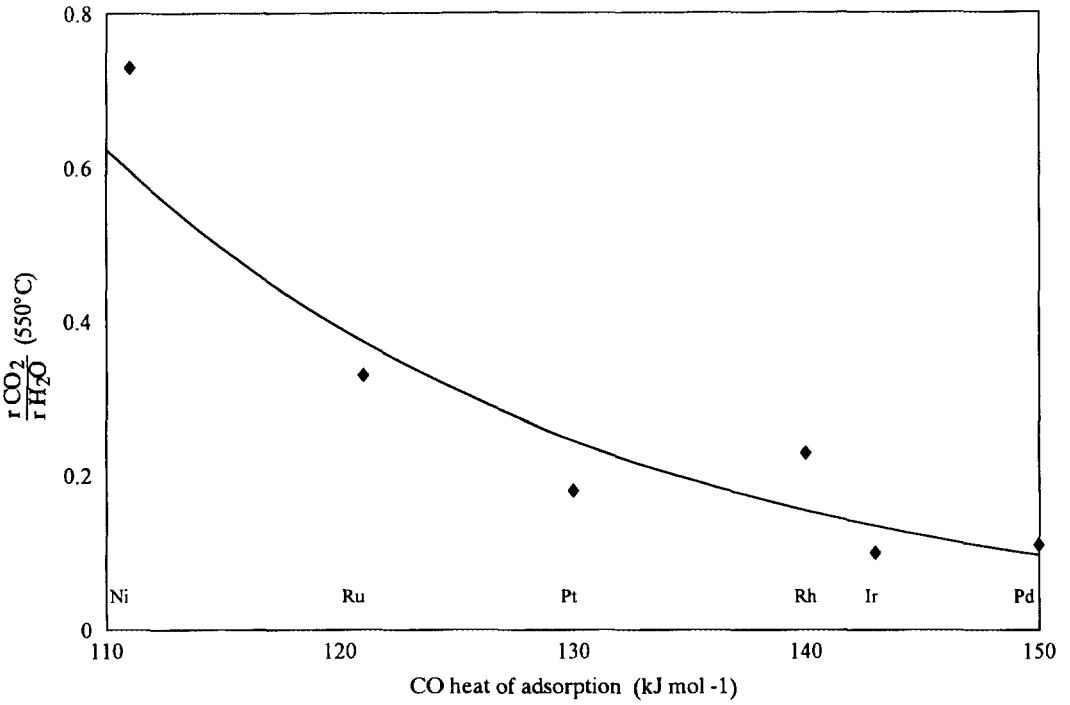

FIG. 7. Relative rates of CO_2 and steam reforming and heat of chemisorption of carbon monoxide.

ity for carbon-free operation. The results on the sulfur-passivated nickel catalysts are in line with earlier observations (*15*). The high selectivity observed on rhodium is less obvious in view of the high coking rate at 650°C (Fig. 5).

CONCLUSIONS

Replacement of steam by carbon dioxide in the reforming reaction has no drastic impact on the mechanism. It results in lower reaction rates which most probably can be explained by reaction kinetics. Further studies are required to describe the change in rates, which, however, have little impact on practical reforming operation, where the reverse shift reaction will soon make steam available for the faster steam reforming route. The activity trend observed for steam reforming with ruthenium and rhodium being the most active metals is less pronounced for CO_2-reforming.

All catalysts show smaller equilibrium constants for methane decomposition than calculated on the basis of graphite. For nickel catalysts, this effect has been explained by the contribution from the surface and elastic energy of the carbon structure being related to the nickel crystal size. For noble metals, this effect is even more pronounced. More work is required to study whether this effect can be related to the structure of the carbon deposits on the noble metals.

Rhodium and ruthenium show high selectivity for carbon-free operation. For ruthenium, this can be ascribed to the high reforming activity combined with low carbon growth rates. Similar results can be achieved by a sulfur-passivated nickel catalyst, but to achieve reasonable reforming rates, high operating temperatures are required.

Ruthenium might be considered as a candidate for CO_2-reforming, being preferred in view of its lower price compared to rhodium (by a factor 50–100). However, the availability of ruthenium (annual production:

4 tonnes/year) (*35*) is too low to have a major impact on the total reforming catalyst market.

ACKNOWLEDGMENTS

The authors thank Mrs. Ulla Ebert Pedersen, Ms. Anne-Marie S. Jensen, Mr. Henning Kosack, Mr. Jens Hyldtoft, Mr. Ole Sørensen, and Dr. Poul L. Hansen for assistance in the experimental work.

REFERENCES

1. Rostrup-Nielsen, J. R., *in* "Catalysis, Science and Technology" (J. R. Anderson and M. Boudart, Eds.), Vol. 5, p. 1. Springer, Berlin, 1984.
2. Stal, J. A., Hanson, D. C., Bak Hansen, J.-H., and Undengaard, N. R., *Oil Gas J.* **90**(10), 62 (1992).
3. Töpfer, H. J., *Gas Wasserfach* **117,** 412 (1976).
4. Tenner, S., *Hydrocarbon Process.* **66,** (7), 52 (1987).
5. Ashcroft, A. T., Cheetham, A. K., Green, M. L. H., and Vernon, P. D. F., *Nature* **352,** 225 (1991).
6. *The Economist* **320** (Sept. 14), 102 (1991).
7. Fischer, F., and Tropsch, H., *Brennstoff. Chem.* **3**(9), 39 (1928).
8. Bodrov, I. M., and Apel'baum, L. O., *Kinet. Katal.* **8,** 379 (1967).
9. Bodrov, I. M., Apel'baum, L. O., and Temkin, M. I., *Kinet. Katal.* **5,** 696 (1964).
10. Rostrup-Nielsen, J. R., *Stud. Surf. Sci. Catal.* **36,** 73 (1988).
11. Alstrup, I., *J. Catal.* **109,** 241 (1988).
12. Lobo, L. S., Trimm, D. L., and Figueiredo, J. L., *in* "Proceedings, 5th International Congress on Catalysis, Palm Beach, 1972," Vol. 2, p. 1125. North Holland/American Elsevier, Amsterdam/New York, 1973.
13. Rostrup-Nielsen, J. R., *J. Catal.* **33,** 184 (1974).
14. Rostrup-Nielsen, J. R., *J. Catal.* **31,** 173 (1973).
15. Rostrup-Nielsen, J. R., *J. Catal.* **85,** 31 (1984).
16. Rostrup-Nielsen, J. R., *Stud. Surf. Sci. Catal.* **68,** 85 (1991).
17. Richardson, J. T., and Papipatyadar, S. A., *Appl. Catal.* **61,** 293 (1990).
18. Vernon, P. D. F., Green, M. L. H., Cheetham, A. K. and Ashcroft, A. T., *Catal. Today* **13,** 417 (1992).
19. Perera, J. S. H. Q., Couves, J. W., Sankar, G. and Thomas, J. M., *Catal. Lett.* **11,** 219 (1991).
20. Oudar, J., and Wise, H., "Deactivation and Poisoning of Catalysts," Chap. 1. Dekker, New York, 1985.
21. Bernardo, C. A., Alstrup, I. and Rostrup-Nielsen, J. R., *J. Catal.* **96,** 517 (1985).
22. Rostrup-Nielsen, J. R., *in* "Fouling Science and Technology" (L. F. Melo, R. R. Bott, and C. A. Bernardo, Eds.), p. 405. Kluwer, Dortrecht, 1988.
23. Hansen, P. L., and Sørensen, O., unpublished results.
24. Xu, J., and Froment, G. F., *AIChE J.* **35,** 88 (1989).
25. Gonzales, O. D., and Parravano, G., *J. Amer. Chem. Soc.* **78,** 4533 (1956).
26. Callen, B. W., Griffiths, K., Nortow, P. R., and Harrington, D. A., *J. Am. Chem. Soc.* **96,** 10905 (1992).
27. Alstrup, I., Chorkendorff, I., and Ullmann, S., *Surf. Sci.* **234,** 79 (1990).
28. Alstrup, I., and Tavares, M. T., *J. Catal.* **135,** 147 (1992).
29. Vannice, M. A., *J. Catal.* **50,** 228 (1977).
30. Campuzano, J. C., *in* "The Chemical Physics of Solid Surfaces and Heterogeneous Catalysis" (D. A. King and D. P. Woodruff, Eds.), Vol. 3, p. 389. Elsevier, Amsterdam, 1990.
31. Baker, R. T. K., and Chludziushi, J. J., *J. Phys. Chem.* **90,** 4734 (1986).
32. Owens, W. T., Rodriguez, N. M., and Baker, R. T. K., *J. Phys. Chem.* **96,** 5048 (1992).
33. Ziemecki, S. B., and Jones, G. A., *J. Catal.* **95,** 621 (1985).
34. Ziemecki, S. B., *Stud. Surf. Sci. Catal.* **38,** 625 (1987).
35. "Platinum 1992." Johnson–Matthey, London, 1992.